IEEE Access
Multidisciplinary ⋮ Rapid Review ⋮ Open Access Journal

Received August 25, 2021, accepted September 14, 2021, date of publication September 20, 2021,
date of current version September 28, 2021.

*Digital Object Identifier 10.1109/ACCESS.2021.3114383*

# On the Investigation of Interface Defects of Solar Cells: Lead-Based vs Lead-Free Perovskite

**MARWA SAYED SALEM BASYONI[1,2], MOSTAFA M. SALAH[3], MOHAMED MOUSA[3], AHMED SHAKER[4], ABDELHALIM ZEKRY[4], (Member, IEEE), MOHAMED ABOUELATTA[4], MOHAMMAD T. ALSHAMMARI[5], KAWTHER A. AL-DHLAN[5], AND CHRISTIAN GONTRAND[6,7]**

[1]Department of Computer Engineering, College of Computer Science and Engineering, University of Ha'il, Ha'il 2240, Saudi Arabia
[2]Department of Electrical Communication and Electronics Systems Engineering, Faculty of Engineering, Modern Science and Arts University, Cairo 12451, Egypt
[3]Electrical Engineering Department, Future University in Egypt, Cairo 11835, Egypt
[4]Faculty of Engineering, Ain Shams University, Cairo 11517, Egypt
[5]Department of Computer Science and Information, Computer Science and Engineering College, University of Ha'il, Ha'il 2240, Saudi Arabia
[6]National Institute of Applied Sciences of Lyon (INSA Lyon), 69621 Villeurbanne, France
[7]IEP, INSA—Fès, Université Euro-Méditerranéenne de Fès, Fès 30120, Morocco

Corresponding author: Ahmed Shaker (ahmed.shaker@eng.asu.edu.eg)

This work was supported by the Deanship of Scientific Research, University of Ha'il, under Project RG-21 023.

**ABSTRACT** Perovskite solar cells (PSCs) have drawn significant consideration as a competing solar cell technology because of the drastic advance in their power conversion efficiency (PCE) over the last two decades. The interfaces between the electron transport layer (ETL) and the absorber layer and between the absorber layer and the hole transport layer (HTL) have a major impact on the performance of the PSCs. In this paper, we have investigated the defect interfaces between ETL/absorber layer and absorber layer/HTL of calibrated experimental $CH_3NH_3PbX_3$ lead-based and $FASnI_3$ lead-free PSCs. The influence of the defect interfaces is studied in order to find the optimum value for the maximum possible PCE. While the PCE has not been enhanced considerably for the lead-based, it is boosted from 1.76% to 5.35% for lead-free PSCs. Also, bulk traps were found to have minor role in comparison with interface traps for the lead-free cell while they have a significant impact for the lead-based cell. The results presented in this work would shed some light on designing interface defects of various types of practical PSC structures and demonstrates the crucial impact of the interface defects on lead-free vs lead-based PSCs. All simulation studies are performed by using SCAPS-1D simulator.

**INDEX TERMS** Interface defects, lead based perovskite solar cell, lead free perovskite solar cell, SCAPS-1D.

## I. INTRODUCTION

Recently, an urgent demand for the substitution of fossil fuels by clean energy sources is universally considered. Solar energy is one of the most best replacement renewable energy resources [1]. Silicon solar cells demonstrate about 90% of the solar cells market [2], [3]. Silicon solar cells offer high PCEs above 25%; however, these cells are suffering from the relatively high cost of fabrication. Consequently, efficient, and low-cost solar cells (SCs) are required [2]. In this regard, perovskite solar cells (PSCs) have been introduced because of their high PCE and low-cost fabrication methods [4]. PSCs have an exceptionally electronic properties like bandgap tunability, low-cost fabrication techniques, wide absorption spectrum and long diffusion lengths of carriers.

Perovskite materials are materials with $ABX_3$ structure where $ABX_3$ is the structure of calcium titanium oxide ($CaTiO_3$). During the years 2009 to 2016, PSCs fabricated from methylammonium lead halides ($CH_3NH_3PbX_3$, where X = Iodine (I), Bromine (Br), or Chlorine (Cl)) have a fast improvement in PCE from 3.8% to more than 22% [5]–[7]. Although this high PCE of lead-based PSCs, toxicity of lead has a severe issue. Two methods are used to alleviate toxicity of lead-based PSCs. Firstly, mixing lead with other metals like tin $CH_3NH_3Sn_xPb_{1-x}$ [8]. Secondly, replace lead with analogous metals. The innocuous Tin is considered the most appropriate material to replace lead because the two materials are from the same group in the periodic table. Tin-based devices suffer from instability and $SnF_2$ is added to

The associate editor coordinating the review of this manuscript and approving it for publication was Cheng Chin.

make the system more stable [9]. Formamidinium tin iodide ($HC(NH_2)_2SnI_3 = FASnI_3$) has been used to make the perovskites more solid and stable. $FASnI_3$ has an energy gap ($E_g$) of 1.41 eV and wide spectrum up to 880 nm. Lately, many methodologies have been proposed to enhance the performance of solar cells based on $FASnI_3$. Using $SnF_2$-pyrazine composite or an inverse are achieved *PCE* of 4.8% and 6.22%, respectively [10], [11]. The open circuit voltage is increased when using cascaded electron transport materials (ETMs) ($TiO_2$–ZnS) [12]. $TiO_2$ and Spiro-OMeTAD are the most famous ETM and hole transport material (HTM), respectively. Other materials like ZnSe, CdS, ZnS, ZnO and ZnOS are used as ETMs and $CsSnI_3$, CuI, $Cu_2O$, CuO, CuSCN and NiO are used as HTMs along with other organic materials [5], [12]–[15].

The interfaces between electron transport layer/perovskite and perovskite/hole transport layer are known as crucial factors for determining the functioning of the perovskite solar cell which also affect the stability of the cell. In the normal structure PSCs, electron transport layers provide paths for electron extraction and have a crucial effect on the interface defects of the following perovskite layer. Hao Sun *et al.* proposed a method to enhance the conductivity of $TiO_2$ electron transport layer which improves the contact of the $TiO_2$/perovskite interface by using $Na_2S$-doped $TiO_2$ layer. This method results in an efficiency of 21.25% [16]. Another technique to improve perovskite performance up to 19.7% is inserting CsBr buffer layer between $NiO_x$ perovskite and hole transport layer to alleviate the lattice mismatch caused by interface stress [17].

Moreover, to relieve the impact of interface traps, defect passivation strategies have been extensively studied [18], [19]. Passivation involves terminating dangling bonds so as to eliminate the recombination centers either within the crystals or on the surfaces. In perovskite materials, several organic molecules have been used, which are demonstrated to improve the open circuit voltage [20]. It was verified that the presence of PbS [21] or C60 [22] passivates the interface and grain boundary defects, and, as a result, reduces the nonradiative recombination. Another technique is performed by using a triple passivation of the two in-between surfaces of the perovskite and hole transport layer by using inorganic salt of Potassium thiocyanate. This improves both the stability and device performance with a record of 21.23% efficiency [23].

A lot of work has been devoted to study the bulk defects and their impact on the solar cell performance [24]–[27]; however, very little efforts were directed to study the interface defects between the different layers of the cell [16], [17], [28], [29]. In this work, we have investigated thoroughly the influence of the interface defects on the performance of lead-based and lead-free PSCs. The study shows the crucial role of this type of defects that govern the performance of the solar cell. In this current study, firstly, we calibrated our simulation vs practical published lead-based and lead-free PSCs using SCAPS-1D simulator. Then, we investigated the defect interfaces ETL/absorber layer and absorber layer /HTL in order to get the maximum possible PCE taking the practical values of defects into consideration. In optimizing the efficiency, we investigate the impact of defect density, energy position with respect to reference level, capture cross-section area of electrons and holes.

## II. CALIBRATION OF THE LEAD BASED AND LEAD-FREE PEROVSKITE SOLAR CELLS

Before studying the impact of interface defects on the performance of the $CH_3NH_3PbX_3$ lead-based solar cell and $FASnI_3$ lead-free PSC, a calibration step is performed. SCAPS-1D is verified with practical lead-based and lead-free PSCs with a design of (Au) as a back contact, ZnO as ETL for the lead-based PSC, $TiO_2$ as ETL for the lead-free PSC, absorber perovskite layer, Spiro-OMeTAD as HTL and Fluorine-doped tin oxide (FTO) as a transparent conducting oxide (TCO) [30], [31]. The calibration is done by taking the given materials parameters from the practical papers and perform the simulations with the same practical parameters [30], [31]. For the other parameters, it is taken from well-known publications as cited in Tables 1 and 2. Finally, comparing the *J-V* curves and the output performance parameters of the simulated cells with the practical cells to ensure the simulation validity. A temperature of 300 K and air mass (AM 1.5) illumination spectrum have been used for all simulations. The $CH_3NH_3PbX_3$ absorption coefficient ($\alpha$) is extracted from practical results [32]. A neutral defect type with Gaussian distribution is chosen to achieve practical data [24]. Equation (1) is used for the calculations of the absorption coefficients ($\alpha$) of TCO, ETM, $FASnI_3$ and HTM with a pre-factor ($A_\alpha$) which is selected to be $10^5$ $cm^{-1}$ $eV^{-1/2}$ [33],

$$\alpha\,(E) = A_\alpha \sqrt{h\nu - E_g} \tag{1}$$

The main structure and the energy band diagram of the PSC different layers are demonstrated in Fig. 1(a) and Fig. 1(b), respectively. The material parameters of SCAPS-1D are listed in Table 1 while Table 2 shows the various defect properties and their parameters. $FASnI_3$ has a p-type charge carrier density [11]. The bulk defect density in $FASnI_3$ is selected to be $2 \times 10^{15}$ $cm^{-3}$ to get a carrier lifetime of 2.5 ns which match the theoretical range (1 ns- 4 ns) [46], [47]. For the lead-based cell a flat band model is utilized for the interfaces TCO/semiconductor and metal/semiconductor. The work functions of TCO and Au for the lead-free cell are set to 4 and 5.1 eV, respectively. Also, the bulk defect density is adjusted at $7 \times 10^{13}$ $cm^{-3}$ to give the best fit with experimental results. Further, the series resistance is estimated to be 5.4 $\Omega.cm^2$ [26]. Fig. 2 demonstrates the J-V curves of the practical PSCs [30], [31] against the simulated cells of the lead-based PSC (Fig. 2(a)) and the lead-free PSC (Fig. 2(b)). The performance parameters of the simulated cells and the practical work are listed in Table 3 showing good accuracy with absolute errors between measurements and simulations less than 5%.

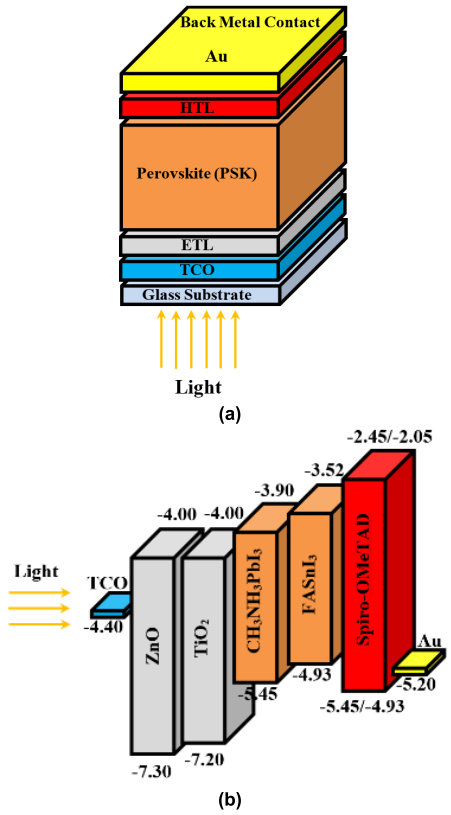


**FIGURE 1.** (a) A generic device structure for PSC and (b) Energy diagrams of ETL (ZnO or $TiO_2$), active layer ($CH_3NH_3PbI_3$ or $FASnI_3$) and HTL (Spiro-OMeTAD).

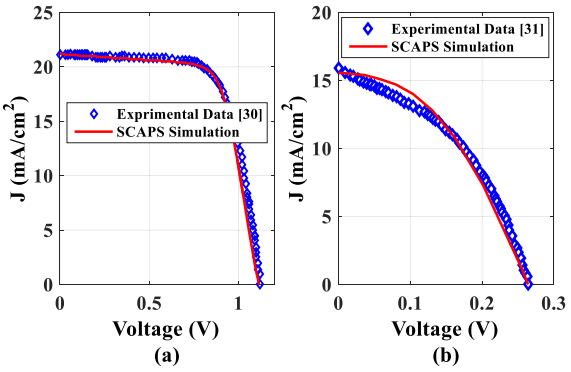


**FIGURE 2.** Calibration of practical PSCs utilizing SCAPS-1D (a) Lead-based PSC and (b) Lead-free PSC.

## III. NUMERICAL TECHNIQUE USED IN SCAPS-1D

Simulation tools are valuable methods for design, studying and expecting the efficiency of SCs. Moreover, simulation tools can help optimize various technological and geometric parameters of solar cells. SCAPS-1D is a useful program to design and study various types of SCs which has been widely verified vs experimental SCs. It can simulate SCs with up to seven layers. Most materials parameters can be assigned such as thickness, energy gap, affinity, permittivity, mobility, and concentration of doping and other physical or geometrical parameters [48]–[50].

**TABLE 1.** Materials parameters of the lead-based and lead-free PSCs.

| Parameters | FTO | ZnO | $TiO_2$ | $MAPbI_3$ | $FASnI_3$ | Spiro-OMeTAD |
|---|---|---|---|---|---|---|
| Thickness (nm) | 500 | 500 | 30 | 400 | 350 | 200 |
| $E_g$ (eV) | 3.5 | 3.3[35] | 3.2[34] | 1.57[25] | 1.41[28] | 3[26, 44] |
| Electron affinity (eV) | 4 | 4[35] | 4[38] | 3.9[40] | 3.52[41] | 2.45[37, 44] |
| Relative permittivity | 9 | 9[35] | 9[35] | 18[40] | 8.2[42] | 3[41] |
| Effective conduction band density $N_c$ ($cm^{-3}$) | $2.2\times10^{18}$ | $2.2\times10^{18}$ | $2\times10^{18}$ | $2.2\times10^{18}$ | $10^{18}$ | $2.2\times10^{18}$ |
| Effective valence band density $N_v$ ($cm^{-3}$) | $1.8\times10^{19}$ | $1.9\times10^{19}$ | $1.8\times10^{19}$ | $1.9\times10^{19}$ | $10^{18}$ | $1.9\times10^{19}$ |
| Thermal velocity of electrons $v_{th,n}$ (cm/s) | $10^7$[34] | $10^7$[34] | $10^7$[34] | $10^7$[34] | $10^7$[34] | $10^7$[34] |
| Thermal velocity of holes $v_{th,p}$ (cm/s) | $10^7$[34] | $10^7$[34] | $10^7$[34] | $10^7$[34] | $10^7$[34] | $10^7$[34] |
| Electron mobility $\mu_e$ ($cm^{-2}\,V^{-1}s^{-1}$) | 20 | 100[35] | 20[37] | 3[40] | 22[43] | $2\times10^{-4}$[44] |
| Hole mobility $\mu_p$ ($cm^{-2}\,V^{-}\,s^{-1}$) | 10 | 25[35] | 10[37] | 17[40] | 22[43] | $2\times10^{-4}$[44] |
| Acceptor concentration $N_A$ ($cm^{-3}$) | 0 | 0 | 0 | 0 | $7\times10^{16}$ | $10^{18}$[37, 39] |
| Donor concentration $N_D$ ($cm^{-3}$) | $2\times10^{19}$ | $10^{18}$ | $9\times10^{16}$ | 0 | 0 | 0 |
| $N_t$ ($cm^{-3}$) | $10^{15}$ | $10^{15}$[36] | $10^{15}$[39] | $7\times10^{13}$ | $2\times10^{15}$ | $10^{15}$[32] |

**TABLE 2.** Parameters of defect interfaces.

| Parameters | ETL/ absorber layer | absorber layer /HTL |
|---|---|---|
| Defect type | neutral[42] | neutral[42] |
| Electrons capture cross section ($cm^2$) | $10^{-15}$[45] | $10^{-15}$[45] |
| Holes capture cross section ($cm^2$) | $10^{-15}$[45] | $10^{-15}$[45] |
| Energetic distribution | Single[45] | Single[45] |
| Reference for defect energy level $E_t$ | Above Highest $E_V$[45] | Above Highest $E_V$[45] |
| Energy level with respect to Reference (eV) | 0.6[45] | 0.6[45] |
| Total density (integrated over all energies) ($1/cm^2$) Lead-based | $10^{11}$ | $10^{11}$ |
| Total density (integrated over all energies) ($1/cm^2$) Lead-free | $10^{16}$ | $10^{16}$ |

**TABLE 3.** Comparison between practical lead-based and lead-free PSCs vs the simulated cells using SCAPS-1D.

| Parameters | | $V_{oc}$ (V) | $J_{sc}$ ($mA/cm^2$) | *FF* (%) | *PCE* (%) |
|---|---|---|---|---|---|
| Lead-based PSCs | Experimental data [30] | 1.120 | 21.13 | 69.68 | 16.60 |
| | Simulated data | 1.114 | 21.17 | 70.03 | 16.53 |
| Lead-free PSCs | Experimental data [31] | 0.264 | 15.85 | 42.00 | 1.75 |
| | Simulated data | 0.2649 | 15.607 | 42.59 | 1.76 |

The numerical solution in SCAPS-1D solves the basic physical differential equations in steady state. The main equations are the continuity equations (Eq. 2 and 3) and Poisson equation (Eq. 4) which are solved self consistently until

convergence occurs.

$$\frac{1}{q}\frac{dJ_n}{dx} = U_n - G(x) \tag{2}$$

$$\frac{1}{q}\frac{dJ_p}{dx} = G(x) - U_p \tag{3}$$

$$\frac{d^2\psi}{dx^2} = \frac{q}{\varepsilon}(n - p + N_A^- - N_D^+ + n_t - p_t) \tag{4}$$

where $G(x)$ is carrier generation rate, generated from the sun, at a distance $x$ below the surface which is given by [51], [52],

$$\begin{aligned} G(x) &= \int_0^{\infty} G(\lambda, x)\, d\lambda \\ &= \int_{\lambda 1}^{\lambda 2} \alpha(\lambda).(1 - r(\lambda)) \cdot N(\lambda, 0) \\ &\quad \cdot Q(\lambda) \cdot e^{[-\alpha(\lambda)\cdot x]} d\lambda \end{aligned} \tag{5}$$

Moreover, the recombination through deep traps in $E_g$ is modeled by the Shockley Read Hall (SRH) model [53], [54]. The SRH recombination for bulk and interface defects is defined by bulk minority carrier lifetimes ($\tau_n$ and $\tau_p$) and interface recombination velocities ($S_n$ and $S_p$), respectively, utilizing the following equations,

$$R_{RSH,bulk} = \frac{(np - n_i^2)}{\tau_p(n + n_1) + \tau_n(p + p_1)} \tag{6}$$

$$R_{RSH,interface} = \frac{(n_{if}p_{if} - n_i^2)}{\frac{p_{if}+p_1}{S_n} + \frac{n_{if}+n_1}{S_p}} \tag{7}$$

$$n_1 = n_i \exp\left(\frac{E_T - E_i}{K_B T}\right) \tag{8}$$

$$p_1 = n_i \exp\left(\frac{E_i - E_T}{K_B T}\right) \tag{9}$$

$$\tau_n = \frac{1}{\sigma_n N_{tB} v_{th}} \tag{10}$$

$$\tau_p = \frac{1}{\sigma_p N_{tB} v_{th}} \tag{11}$$

$$S_n = \sigma_n N_t v_{th} \tag{12}$$

$$S_p = \sigma_p N_t v_{th} \tag{13}$$

The symbols used in the aforementioned equations along with their definitions are summarized in Table 4.

Fig. 3 illustrates a flow chart of the numerical solution of SCAPS-1D. Firstly, the cell geometry is inserted. Then, the materials parameters are defined. Poisson equation and continuity equations are discretized into different mesh points. Discretization is executed by implying the finite difference method (FEM), and the current densities are modeled using the Scharfetter–Gummel process [55]. In the assigned mesh points, $\psi$, $n$ and $p$ are iteratively computed by the Gummel method [56]. Physical models such as *G, U,* $\mu_n$ and $\mu_p$ are enhanced after each iteration. Finally, we can get *J-V, C-V, C-F, QE, AC, G, U* and energy diagrams [57].

In should be emphasized here that, in SCAPS-1D, an interface can be studied between any two layers. The model used for this implementation is thermionic emission. The thermal velocity in an interface is equal to the least thermal velocity of the two layers. The interface defects could be treated like bulk defects. The recombination in interface states is evaluated by the Pauwels-Vanhoutte theory [58], which is an extension of the SRH theory.

The traps act as recombination centers lead to losses in the photocurrent and an increase in the dark current. Both effects contribute to the decrease in the photo conversion efficiency. The key physical parameters that ascertain how a

**TABLE 4. Definition of physical quantities used in SCAPS simulator.**

| Symbol | Definition | Unit |
|---|---|---|
| $q$ | Electron charge | C |
| $\varepsilon$ | Permittivity of the materials of the different layers | F/cm |
| $J_n$ and $J_p$ | Electron and hole current densities, respectively. They are calculated based on the drift-diffusion model | A/cm$^2$ |
| $U_n$ and $U_p$ | Electron and hole recombination rate. This includes Auger, radiative, deep traps, and impact ionization. | cm$^{-3}$s$^{-1}$ |
| $\psi$ | Electrostatic potential | V |
| $N_D^+$ and $N_A^-$ | Shallow donor and acceptor ionized concentrations | cm$^{-3}$ |
| $n_t$ and $p_t$ | Trapped electron and hole concentrations | cm$^{-3}$ |
| $n$ and $p$ | Electron and hole densities | cm$^{-3}$ |
| $N_{tB}$ and $N_t$ | Bulk and interface defect density | cm$^{-3}$ |
| $\sigma_n$ and $\sigma_p$ | Electron and hole capture cross-section | cm$^2$ |
| $S_n$ and $S_p$ | Electron and hole surface recombination velocity | cm/s |
| $E_t$ | Trap energy level | eV |
| $\lambda_1$ and $\lambda_2$ | lower and upper limits of the wavelengths of absorbed photons, respectively | μm |
| $\alpha(\lambda)$ and $r(\lambda)$ | the absorption coefficient and reflection coefficient, respectively | cm$^{-1}$ |
| $Q(\lambda)$ | Internal quantum efficiency | |
| $N(\lambda, 0)$ | incident photon flux | Photons/ s.m$^2$ |

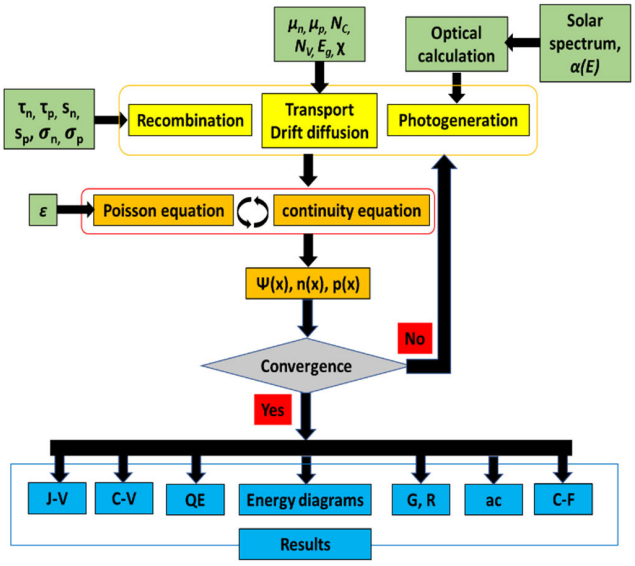


**FIGURE 3. Flow chart of the numerical solutions in SCAPS-1D.**

specific trap affects the nonradiative recombination rate are the trap density, energy level, and electron and hole capture cross sections. Regarding the density $N_t$, its value can be technologically controlled by reducing the crystallographic defects as grain boundaries and surface defects at the interfaces throughout the fabrication processes [28].

The electron and hole capture cross sections depend mainly on the static dielectric constant of the material [59]. Also, they depend on the physical and chemical uniqueness of the trap and more prominently on the trap charge state. If the dielectric constant is high, the screening is strong, and it is less likely that a charge becomes captured. In [60], it was shown the liquid-like molecular reorientation motions in the perovskite allow the effective carrier screening. In addition, in [61], the potassium halide species at the grain boundaries was observed to lower the capture cross section.

It is reported that neutral vacancy pairs and elementary vacancy defects do not create deep energy states inside the perovskite bandgap. Only shallow traps are most likely generated which are not anticipated to act as powerful recombination centers [62]. Further, some impurities in the $PbI_2$ precursor and traces of Au in the perovskite layer, resulting from electrode diffusion, have been reported to decrease the cell performance [63]. The trap energy levels could also be affected by whether the perovskite layer is p-type or n-type [64]. So, to avoid such impurities which may produce deep traps, careful manufacturing processes and tuning the film composition and morphology are required.

In the following sections, we will study the impact of each interface parameters to determine the most important parameters that can be tuned to get the best performance. Also, the impact of bulk traps on the performance will be investigated to give a complete picture of the traps effect and to demonstrate the dominant traps the have the most significant role in controlling the efficiency of the lead-based and lead-free PSCs.

## IV. OPTIMIZATION OF ETL/PSK AND PSK/HTL DEFECT INTERFACES OF THE LEAD BASED CELL

### A. OPTIMIZATION OF ETL/PSK DEFECT INTERFACE

In this subsection, the influence of defect density $N_t$ between ETL and perovskite interface is studied. It has a substantial impact on the functioning of the solar cell as the quality of the interface ETL/absorber layer has shown a pronounced influence on the performance of the PSC [65]. Consequently, the recombination rate of carriers increases which alters $V_{oc}$ of the PSC. Fig. 4(a) illustrates the efficiency vs interface defect density where the computation is based on the Fermi level ($E_{fn}$). The performance is improved with reducing $N_t$ with no considerable impact below $N_t$ of $1 \times 10^{11}$ cm$^{-2}$. As lowering $N_t$ means increasing the cost of fabrication, a value of $N_t$ of $1 \times 10^{11}$ cm$^{-2}$ could be chosen as a design parameter which gives $PCE = 16.53\%$.

In the next simulations, two distinct values of $N_t$ are used: a low concentration value of $10^{11}$ cm$^{-2}$ and a high concentration value of $10^{14}$ cm$^{-2}$. The variation of the defect

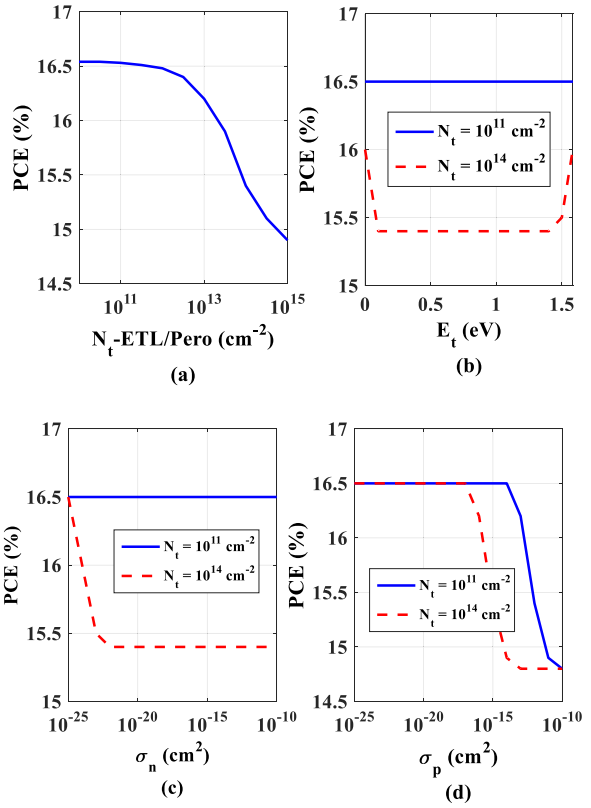


**FIGURE 4.** Variation in efficiency according to the variation of (a) $N_t$ of the ETL/Perovskite interface, (b) $E_t$-$E_{Vmax}$, (c) $\sigma_n$ and (d) $\sigma_p$.

position ($E_t$) with respect to the highest $E_V$ is inspected. It can be inferred from Fig. 4(b) that the change of $E_t$ does not affect the PCE for the low value of $N_t$. On the other hand, for the high concentration value of $N_t$, the PCE starts with a high value of about 16% when $E_t$ coincides with the valence band edge, $E_v$, then it has a lower constant value of 15.41% up to the defect position, $E_t$ of 1.3 eV. The PCE is then increased reaching about 16% for $E_t$ matched with the conduction band edge, $E_c$. There are two types of defects; the shallow defects with position of higher and lower than the mid of the $E_g$ of PSK and nearer to $E_c$ and $E_v$, respectively which have low destructive impact on performance in comparison to deep defects which are near the mid of $E_g$ [66].

In addition, the PCE variation vs ETL/PSK cross-section area of electrons ($\sigma_n$) is investigated for the same two levels of $N_t$. As discussed herein, the capture cross-section signifies the likelihood of the trap capturing the free charge carrier. When light is irradiated to the PSC, carriers are generated in the absorber layer [36]. The electrons will be in the direction from the absorber layer to ETL and the holes will be in the direction from the absorber layer to HTL. Consequently, in ETL/PSK interface the cross-section area of electrons has no significant effect upon the performance parameters and the cross-section area of holes has a significant impact. However, in the PSK/HTL interface the cross-section area of electrons has significant influence on the performance parameters and the cross-section area of holes has no significant impact.

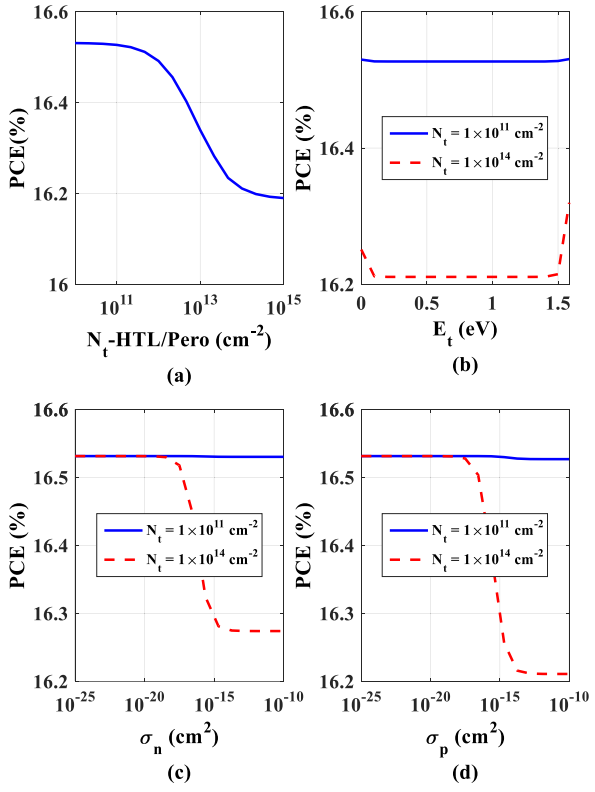


**FIGURE 5.** Variation in efficiency according to the variation of (a) $N_t$ of the HTL/Perovskite interface, (b) $E_t$-$E_{Vmax}$, (c) $\sigma_n$ and (d) $\sigma_p$.

So, the PCE dependence on $\sigma_n$ is the same as the previous calculations. It can be inferred from Fig. 4(c) that the change of $\sigma_n$ does not affect the PCE for the low value of $N_t$. But for the large value of $N_t$, the PCE is decreasing with increasing the capture cross section, $\sigma_n$. The PCE is about 15.45% for $\sigma_n$ greater than $1 \times 10^{-22}$ cm$^2$. For $N_t$ of $10^{11}$ cm$^{-2}$, $\sigma_n$ of $1 \times 10^{-15}$cm$^2$ is chosen as a practical value.

Furthermore, the effect of ETL/PSK cross-section area of holes ($\sigma_p$) is investigated. Fig. 4(d) illustrates the efficiency vs $\sigma_p$. Increasing the cross-section has a significant impact on the performance. For $N_t$ of $10^{11}$ cm$^{-2}$, the PCE is decreasing for $\sigma_p$ greater than $1 \times 10^{-14}$ cm$^2$ but for $N_t$ of $10^{14}$ cm$^{-2}$, the PCE is decreasing for $\sigma_p$ greater than $1 \times 10^{-18}$ cm$^2$. So, $\sigma_p$ of $1 \times 10^{-16}$ cm$^2$ may be chosen.

### B. OPTIMIZATION OF PSK/HTL DEFECT INTERFACE

Here, the defect density of the absorber/HTL interface is investigated. Fig. 5(a) illustrates the PCE variation vs interface defect density where the calculation is based on the Fermi level ($E_{fp}$). The efficiency is improved with lowering $N_t$ with no major impact below $N_t$ of $1 \times 10^{11}$ cm$^{-2}$. $N_t$ of $1 \times 10^{11}$ cm$^{-2}$ is chosen and, in this case, PCE = 16.53%.

Next, two values of $N_t$ are treated, $10^{11}$ cm$^{-2}$ and $10^{14}$ cm$^{-2}$. For the low concentration value of $N_t$, the energy $E_t$ with respect to the highest $E_V$ and $\sigma_p$ of absorber/HTL interface does not have a significant impact on the performance as can be depicted in Fig. 5(b) and Fig. 5(d), respectively, while an efficiency degradation is observed when PSK/HTL cross-section area of electrons ($\sigma_n$) is increased as can be depicted in Fig. 5(b). Meanwhile, for the other high concentration value of $N_t$, the trend of the impact of trap energy position, illustrated in Fig. 5(b), is the same as that of the ETL/Perovskite interface which indicates the crucial role of designing shallow acceptor traps (near $E_c$) to enhance the cell performance for any trap density value. Furthermore, the efficiency degradation is observed when PSK/HTL cross-section area of electrons and holes are increased as can be depicted in Fig. 5(c) and Fig. 5(d), respectively. Values of $\sigma_n = 1 \times 10^{-15}$ cm$^2$ and $\sigma_p = 1 \times 10^{-15}$cm$^2$ could be chosen to prevent this degradation.

It can be concluded here that the most vital factor that affects the performance of the cell is the trap density. If the trap density is low, the impact of $E_t$ position is neglected while there is a minor influence on the efficiency when concerning $\sigma_p$ for the ETL/Perovskite interface and $\sigma_n$ for the HTL/Perovskite interface. This is due to the rise of the electron and hole surface recombination velocity according to increasing $\sigma_n$ or $\sigma_p$ as indicated in Eq. (12) and Eq. (13). As $N_t$ increases, the impact of $N_t$ on the efficiency is more noticeable and one can see the importance of refining the design parameters in order to reach an optimum cell performance.

## V. OPTIMIZATION OF ETL/PSK AND PSK/HTL INTERFACE DEFECTS OF THE LEAD-FREE CELL

In this section, we study the influence of the defect interfaces between ETL/PSK and PSK/HTL of the lead-free PSC. The sequence of the optimization is carried out in the same order as in the case of lead-based PSC.

### A. OPTIMIZATION OF ETL/PSK INTERFACE DEFECT

The variation of the interface defect density of the interface ETL/absorber layer is investigated in Fig. 6(a) which illustrates the impact of the interface defect density on PCE. The performance is improved with decreasing $N_t$ with no lower limit according to the simulation. This finding is extremely important as the trend is not the same as the lead-based cells. In lead-based PSC, there is a lower limit for the trap density below which there is no significant improvement in the efficiency. On the other hand, in lead-free PSC, decreasing trap density gives a linear increase in the efficiency which is beneficial in solar cell design. But as lowering $N_t$ means increasing the cost of fabrication, a suitable value $N_t$ of around $4 \times 10^{11}$ cm$^{-2}$ could be chosen in our design which gives PCE = 4.5%.

Two values of $N_t$ are used in the investigation of the influence of trap parameters on the efficiency. A low concentration value of $4 \times 10^{11}$ cm$^{-3}$ and a high concentration value of $10^{14}$ cm$^{-3}$ are considered in the following simulations. The effect of ETL/PSK trap energy position ($E_t$) with respect to the highest $E_V$ is firstly studied as shown in Fig. 6(b). For low value of $N_t$, the change of $E_t$ does not affect the PCE substantially. when $N_t$ is $10^{14}$ cm$^{-3}$, the PCE is degraded if the trap position is near the mid-gap. So, for both cases of trap density, $E_t$ is chosen to be a shallow trap in order to boost

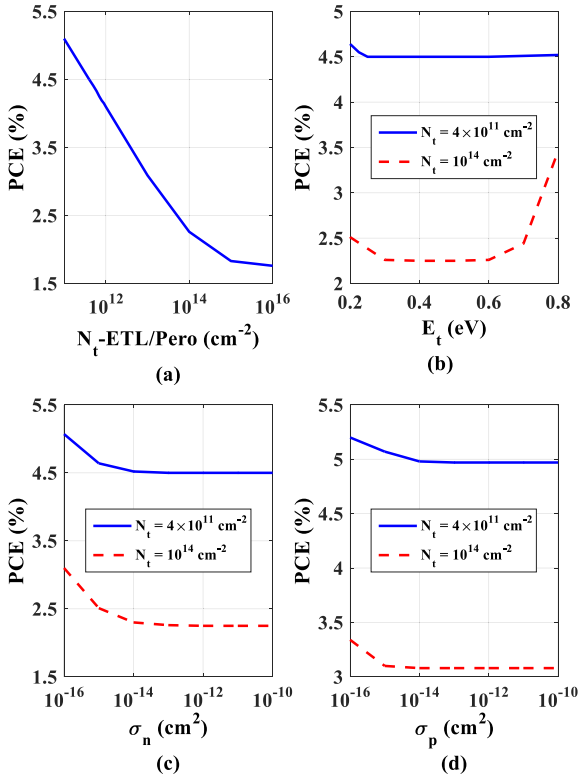


**FIGURE 6.** Variation in PCE according to the variation of (a) $N_t$ of ETL/Perovskite interface, (b) $E_t$-$E_{Vmax}$, (c) $\sigma_n$ and (d) $\sigma_p$.

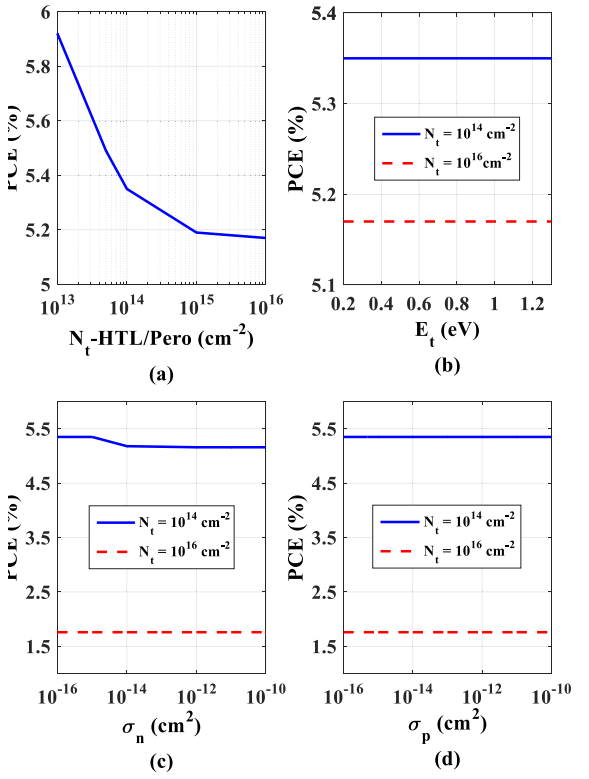


**FIGURE 7.** Variation in PCE according to the variation of (a) $N_t$ of HTL/Perovskite Interface, (b) $E_t$-$E_{Vmax}$, (c) $\sigma_n$ and (d) $\sigma_p$.

the performance. In addition, the impact of ETL/PSK $\sigma_n$ and $\sigma_p$ is examined and the results of the corresponding PCE is shown in Fig. 6(c) and Fig. 6(d), respectively. It is noticed the performance is degraded for low values of $\sigma_n$ and $\sigma_p$ for both values of $N_t$. So, $\sigma_n$ of $1 \times 10^{-16}$ cm$^2$ is chosen. Also, $\sigma_p = 5 \times 10^{-16}$ cm$^2$ is preferable for both trap concentrations.

### B. OPTIMIZATION OF PSK/HTL DEFECT INTERFACE

The variation of the defect density of the absorber/HTL interface is explored as illustrated in Fig. 7(a). The performance is improved with decreasing $N_t$ which is the same trend as for the absorber/ETL interface Two different values of $N_t$ are considered in the next simulations, $1 \times 10^{14}$ cm$^{-3}$ and $10^{16}$ cm$^{-3}$. Fig. 7(b) illustrates the performance variation vs PSK/HTL trap energy position ($E_t$) with respect to the highest $E_V$ (which is that of the PSK). It can be inferred from the figure that the change of $E_t$ does not affect the PCE for any $N_t$ value; so, an $E_t$ position which coincides with $E_c$ or $E_v$ is chosen. Further, Fig. 7(c) and Fig. 7(d) illustrate the dependence of PCE on PSK/HTL $\sigma_n$ and $\sigma_p$ for the two values of $N_t$. the dependence is weak as can be inferred from the figures. $\sigma_n$ of $1 \times 10^{-15}$ cm$^2$ and $\sigma_p$ of $1 \times 10^{-15}$ cm$^2$ are chosen as design parameters.

Also, it can be concluded here, for the lead-free cell, that the most critical factor that influences the cell efficiency is the trap density. If the trap density is low, the impact of $E_t$ position is neglected while there is a minor influence on the efficiency when concerning $\sigma_p$ and $\sigma_n$ for the ETL/Perovskite interface and HTL/Perovskite interface. As $N_t$ increases, the impact of $E_t$ on the efficiency is noticeable only for the ETL/Perovskite interface while it has a minor effect for the HTL/Perovskite interface. Moreover, the impact of $\sigma_p$ and $\sigma_n$ is not strong as in the case of lead-based solar cell. This is due to the higher $N_t$ values encountered in the lead-free cell vs the lead-based one.

## VI. PHYSICAL INTERPRETATION OF THE RESULTS BEFORE AND AFTER OPTIMIZATION

One of the most important differences between the lead-based and lead-free PSCs is the impact of the interface trap density. Regarding the lead-based sell, decreasing $N_t$ beyond a certain value is not beneficial as there is a saturation in the efficiency. However, the efficiency is boosted linearly when decreasing $N_t$ concerning the lead-free cell. Further, shallow defects with a position lower than the mid of $E_g$ of PSK have low destructive effect on performance, while deep defects which are near the mid of $E_g$ have strong influence [39]. This is true for both types of solar cells.

As mentioned above in the lead-based cell, in ETL/PSK interface, for low values of $N_t$, the cross-section area of electrons has no significant effect on the efficiency while the cross-section area of holes has a significant impact. On the other hand, in PSK/HTL interface the cross-section area of electrons has a more substantial impact on the performance than that of the effect of cross-section area of holes. Also, both cross-section areas of electrons and holes in ETL/PSK and

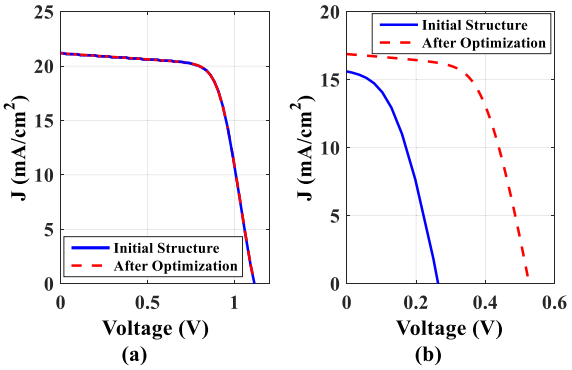


**FIGURE 8.** (a) JV curves of the initial and optimized lead-based cell and (b) JV curves of the initial and optimized lead-free cell.

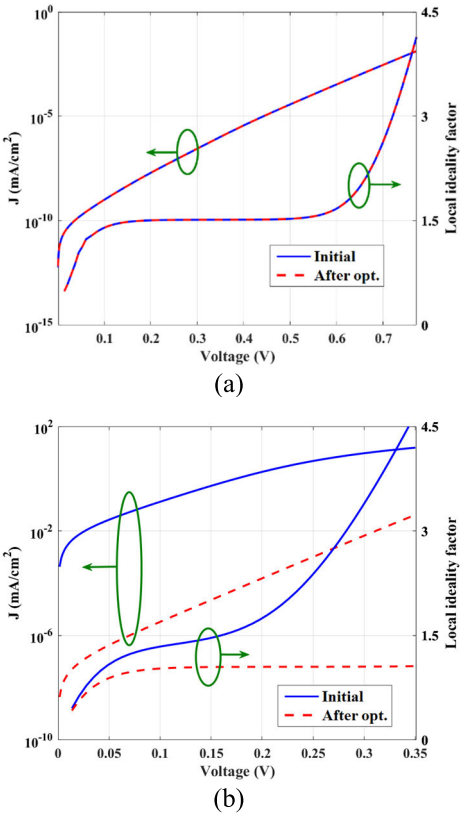


**FIGURE 9.** Dark characteristics before and after optimization of (a) the lead-based cell and (b) the lead-free cell.

PSK/HTL defect interfaces of the lead-free cell have a little influence on the performance parameters. This difference is according to the distinction of the structure of the cells. In the lead-based, an intrinsic layer of perovskite is sandwiched between ETL and HTL and the structure is p-i-n [67]. But in the lead-free cell the structure is $p^{+}$-p-n [26].

In this section, we provide a comparison that demonstrates the effectiveness of the optimization processes of the interfaces carried out in this work for both lead-based and lead-free PSCs. Firstly, the JV curves of the initial and optimized PSCs for the lead-based cell and the lead-free one are simulated and the results are shown in Fig. 8(a) and Fig. 8(b),

**TABLE 5.** Comparison between the initial design and the optimized one.

| | $V_{oc}$ (V) | $J_{sc}$ (mA/cm$^2$) | $FF$ (%) | $PCE$ (%) |
|---|---|---|---|---|
| Initial (Lead-based) | 1.114 | 21.174 | 70.03 | 16.53 |
| Optimized (Lead-based) | 1.115 | 21.175 | 70.02 | 16.53 |
| Initial (Lead-free)) | 0.2649 | 15.607 | 42.59 | 1.76 |
| Optimized (Lead-free) | 0.5259 | 16.727 | 60.84 | 5.35 |

respectively. The performance parameters of the initial design and after optimizing the defect interfaces, for both lead-based and lead-free PSCs, are listed in Table 5 for comparison. The influence of interface parameters on the lead-based is minor and very little improvement is accomplished. However, the design and tuning of the interface parameters significantly affects the performance of the lead-free PSC.

Referring to Table 5, the performance enhancement for the lead-free cell is mainly due to the improvement in the open circuit voltage ($V_{oc}$) which increases from about 0.26 V to about 0.52 V. This doubling of $V_{oc}$ is due to overcoming the recombination mechanism that arises on the interfaces and limit the reverse saturation current of the cell. For a physical justification of the cell behavior corresponding to the interfaces' optimization, we draw the dark characteristics before and after optimization for the lead-based and lead-free cells as shown in Fig. 10(a) and Fig. 10(b), respectively. Also, the local ideality factor is illustrated. As can be inferred from Fig. 10(a), the lead-based cell has almost the same reverse saturation current for both the initial and final structures. Regarding the lead-free cell, the situation is completely different. The reverse saturation current is declined for the optimized design which indicates a higher open circuit voltage. Also, the local ideality factor is decreased which results in a higher fill factor [68], [69]. The low ideality factor results in less recombination losses which was proven experimentally in the literature [70]. So, this work shows the importance of optimization of interface defects on the performance of lead-free PSCs. Most studies are directed to lead-based cells, but their improvements are limited because of the high efficiency of the initial structure. This study is very important because it shows that inspecting the interface defects in the lead-free cells is crucial to increase the cell efficiency.

## VII. BULK TRAPS VS INTERFACE TRAPS

In the previous sections, the interface properties were investigated thoroughly to optimize and determine the most important parameters that strongly impacts the efficiency of the PSC. In this section, we incorporate the bulk traps into our study to give a complete picture about the influence of various types of defects. This analysis is important to determine the most effective competing defects, bulk vs interface traps. The bulk traps that are highly effective in the PSC are those found inside the absorber as it is the region in which the photoexcited carriers are mainly generated.

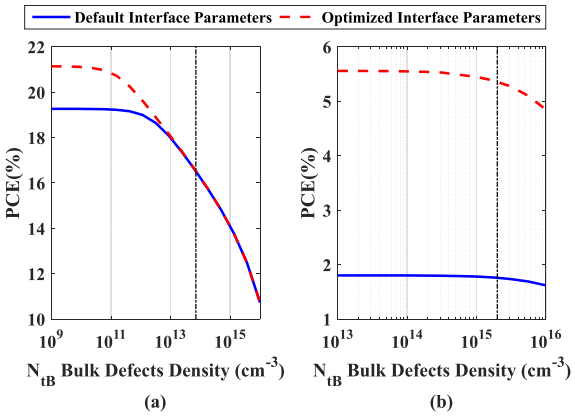


**FIGURE 10. Efficiency of the solar cell utilizing default and optimized interface parameters as a function of bulk defect density (a) lead-based PSC and (b) lead-free PSC. The vertical lines indicate the default bulk trap density used in all other simulations.**

Figure 10 displays the efficiency as a function of absorber bulk trap density $N_{tB}$ for both lead-based (Fig. 10(a)) and lead-free (Fig. 10(b)) PSCs. The simulation is carried out for two cases, one with the default values of the interface parameters and the other case is for optimized parameters designed here before. Generally, the trend of the efficiency is that it increases when the bulk trap density decreases as expected. As displayed in Fig. 10(a), when $N_{tB}$ is lower than $10^{11}$ cm$^{-3}$ in the lead-based cell before optimization of the interface parameters, the efficiency nearly saturates at about 19.25% with any further decrease in $N_{tB}$. Also, when the interface parameters are optimized, the PCE saturates at a higher value, namely about 21.15%. the results show the crucial role of the bulk traps in lead-based cells. Also, the role of interface traps is dominant for low values of $N_{tB}$. So, in order to have a good design for the lead-based PSC, both bulk and interface traps should be optimized simultaneously.

Referring to Fig. 10(b), the efficiency trend, according to the variation of bulk trap density, is less pronounced for the lead-free cell. The PCE increases from 1.76% and saturates at slightly higher than 1.8% for $N_{tB}$ lower than $10^{14}$ cm$^{-3}$. Additionally, for the optimized interface parameters, the PCE increases from 5.35% to 5.55% when $N_{tB}$ decreases from $2 \times 10^{15}$ cm$^{-3}$ to $10^{14}$ cm$^{-3}$. This little increase in the PCE suggests the minor impact of the bulk traps for the lead-free cell. These results show the importance of optimizing the interface parameters in lead-free cells to enhance the efficiency.

## VIII. CONCLUSION

SCAPS-1D is utilized to simulate lead-based PSC with ZnO as ETL and Spiro-OMeTAD as HTL. The lead-based PSC is firstly verified with a practical work. The influence of the interfaces' defects ETL/absorber and absorber/HTL is investigated. Decreasing $N_t$ of ETL/absorber and absorber/HTL interfaces from $1 \times 10^{11}$ to $1 \times 10^{10}$ cm$^{-2}$ increases the PCE by only 0.02%. If $N_t$ is increased, the PCE decreases substantially. Although the interfaces' defects could be optimized, the photovoltaic parameters do not change. In addition, we have calibrated a lead-free PSC with practical measurements. The influence of the interface defects ETL/absorber and absorber/HTL is investigated. Decreasing $N_t$ of ETL/absorber and absorber/HTL interfaces is found to have a pivotal effect leading to increase the efficiency linearly. This impact is not seen in the lead-based cells as the efficiency is saturated beyond a certain value of the trap density. Regarding the lead-free cell, the interface defects are optimized and the PCE is enhanced from 1.76% to 5.35% at a considerably low interface trap density that is not far from experimental considerations.

Other interface parameters like the electron and hole cross-section area, and trap energy position are investigated. For lower values of $N_t$, the influence $\sigma_n$, $\sigma_p$ and $E_t$ is minor on the PCE. On the other hand, for the higher values of $N_t$, the influence is significant, and care must be taken in order to design such factors for better performance. Finally, we investigated the variation of bulk trap density of the absorber to differentiate between its impact on the cell performance and the impact of the interface quality. It was found that the interface influence is much more crucial than the bulk traps specially for the lead-free PSC.

Moreover, the impact of the absorber bulk trap density is investigated. In the lead-based cell, optimizing the interface traps pushes the efficiency for low values of bulk traps. So, both types of traps play important role in controlling the recombination through the PSC. On the other hand, in the case of lead-free cell, the bulk traps have minor influence while the interface quality greatly impacts the performance and is a promising direction to boost the efficiency.

This study successfully addresses the impact of various parameters of interface traps on the performance of PSCs and provides some design guidelines that can help to boost the efficiency of this type of cells. Finally, the presented study sheds the light on two different materials as case studies for the lead-based and lead-free perovskite solar cells. More efforts should be directed to inspect more materials with different bandgaps to optimize their performance under the influence of interface traps.

## REFERENCES

[1] A. Zekry, A. Shaker, and M. Salem, "Solar cells and arrays: Principles, analysis, and design," in *Advances in Renewable Energies and Power Technologies*. Amsterdam, The Netherlands: Elsevier, 2018, pp. 3–56.

[2] N. Qamhieh, A. Najar, Z. N. Qamhieh, B. Abdel Aziz, A. Mansour, and I. Alghoul, "Synthesis and characterization of a perovskite film for solar cells applications," *Optik*, vol. 171, pp. 648–651, Oct. 2018, doi: 10.1016/j.ijleo.2018.05.066.

[3] M. S. Salem, A. J. Alzahrani, R. A. Ramadan, A. Alanazi, A. Shaker, M. Abouelatta, C. Gontrand, M. Elbanna, and A. Zekry, "Physically based analytical model of heavily doped silicon wafers based proposed solar cell microstructure," *IEEE Access*, vol. 8, pp. 138898–138906, 2020, doi: 10.1109/ACCESS.2020.3012657.

[4] P. Gao, M. Grätzel, and M. K. Nazeeruddin, "Organohalide lead perovskites for photovoltaic applications," *Energy Environ. Sci.*, vol. 7, no. 8, pp. 2448–2463, Apr. 2014, doi: 10.1039/c4ee00942h.

[5] M. Hatamvand, S. A. Mirjalili, M. Sharzehee, A. Behjat, M. Jabbari, and M. Skrifvars, "Fabrication parameters of low-temperature ZnO-based hole-transport-free perovskite solar cells," *Optik*, vol. 140, pp. 443–450, Jul. 2017, doi: 10.1016/j.ijleo.2017.02.101.

[6] K. Akihiro, T. Kenjiro, S. Yasuo, and M. Tsutomu, "Organometal halide perovskites as visible-light sensitizers for photovoltaic cells," *J. Amer. Chem. Soc.*, vol. 131, no. 17, pp. 6050–6051, Apr. 2009, doi: 10.1021/ja809598r.

[7] F. Giordano, A. Abate, J. P. Correa Baena, M. Saliba, T. Matsui, S. H. Im, S. M. Zakeeruddin, M. K. Nazeeruddin, A. Hagfeldt, and M. Graetzel, "Enhanced electronic properties in mesoporous $TiO_2$ via lithium doping for high-efficiency perovskite solar cells," *Nature Commun.*, vol. 7, no. 1, pp. 1–6, Apr. 2016, doi: 10.1038/ncomms10379.

[8] Y. Ogomi, A. Morita, S. Tsukamoto, T. Saitho, N. Fujikawa, Q. Shen, T. Toyoda, K. Yoshino, S. S. Pandey, T. Ma, and S. Hayase, "$CH_3NH_3SnxPb(_{1-x})I_3$ perovskite solar cells covering up to 1060 nm," *J. Phys. Chem. Lett.*, vol. 5, no. 6, pp. 1004–1011, Mar. 2014, doi: 10.1021/jz5002117.

[9] A. G. Kontos, A. Kaltzoglou, E. Siranidi, D. Palles, G. K. Angeli, M. K. Arfanis, V. Psycharis, Y. S. Raptis, E. I. Kamitsos, P. N. Trikalitis, C. C. Stoumpos, M. G. Kanatzidis, and P. Falaras, "Structural stability, vibrational properties, and photoluminescence in $CsSnI_3$ perovskite upon the addition of $SnF_2$," *Inorganic Chem.*, vol. 56, no. 1, pp. 84–91, Jan. 2017, doi: 10.1021/acs.inorgchem.6b02318.

[10] S. J. Lee, S. S. Shin, Y. C. Kim, D. Kim, T. K. Ahn, J. H. Noh, J. Seo, and S. I. Seok, "Fabrication of efficient formamidinium tin iodide perovskite solar cells through $SnF_2$–Pyrazine complex," *J. Amer. Chem. Soc.*, vol. 138, no. 12, pp. 3974–3977, Mar. 2016, doi: 10.1021/jacs.6b00142.

[11] W. Liao, D. Zhao, Y. Yu, C. R. Grice, C. Wang, A. J. Cimaroli, P. Schulz, W. Meng, K. Zhu, R. Xiong, and Y. Yan, "Lead-free inverted planar formamidinium tin triiodide perovskite solar cells achieving power conversion efficiencies up to 6.22%," *Adv. Mater.*, vol. 28, no. 42, pp. 9333–9340, Nov. 2016, doi: 10.1002/adma.201602992.

[12] W. Ke, C. C. Stoumpos, J. L. Logsdon, M. R. Wasielewski, Y. Yan, G. Fang, and M. G. Kanatzidis, "$TiO_2$–ZnS cascade electron transport layer for efficient formamidinium tin iodide perovskite solar cells," *J. Amer. Chem. Soc.*, vol. 138, no. 45, pp. 14998–15003, Nov. 2016, doi: 10.1021/jacs.6b08790.

[13] P.-Y. Gu, N. Wang, A. Wu, Z. Wang, M. Tian, Z. Fu, X. W. Sun, and Q. Zhang, "An azaacene derivative as promising electron-transport layer for inverted perovskite solar cells," *Chem. Asian J.*, vol. 11, no. 15, pp. 2135–2138, Aug. 2016, doi: 10.1002/asia.201600856.

[14] A. A. Said, J. Xie, and Q. Zhang, "Recent progress in organic electron transport materials in inverted perovskite solar cells," *Small*, vol. 15, no. 27, Jul. 2019, Art. no. 1900854, doi: 10.1002/smll.201900854.

[15] P.-Y. Gu, N. Wang, C. Wang, Y. Zhou, G. Long, M. Tian, W. Chen, X. W. Sun, M. G. Kanatzidis, and Q. Zhang, "Pushing up the efficiency of planar perovskite solar cells to 18.2% with organic small molecules as the electron transport layer," *J. Mater. Chem. A*, vol. 5, no. 16, pp. 7339–7344, 2017, doi: 10.1039/c7ta01764b.

[16] H. Sun, D. Xie, Z. Song, C. Liang, L. Xu, X. Qu, Y. Yao, D. Li, H. Zhai, K. Zheng, and C. Cui, "Interface defects passivation and conductivity improvement in planar perovskite solar cells using $Na_2S$ doped compact $TiO_2$ electron transport layers," *ACS Appl. Mater. Interface*, vol. 12, no. 20, pp. 22853–22861, 2020, doi: 10.1021/acsami.0c03180.s001.

[17] B. Zhang, J. Su, X. Guo, L. Zhou, Z. Lin, L. Feng, J. Zhang, J. Chang, and Y. Hao, "NiO/perovskite heterojunction contact engineering for highly efficient and stable perovskite solar cells," *Adv. Sci.*, vol. 7, no. 11, Jun. 2020, Art. no. 1903044, doi: 10.1002/advs.201903044.

[18] H. Tan, A. Jain, O. Voznyy, X. Lan, F. P. García de Arquer, J. Z. Fan, R. Quintero-Bermudez, M. Yuan, B. Zhang, Y. Zhao, F. Fan, P. Li, L. N. Quan, Y. Zhao, Z.-H. Lu, Z. Yang, S. Hoogland, and E. H. Sargent, "Efficient and stable solution-processed planar perovskite solar cells via contact passivation," *Science*, vol. 355, no. 6326, pp. 722–726, Feb. 2017, doi: 10.1126/science.aai9081.

[19] X. Zheng, B. Chen, J. Dai, Y. Fang, Y. Bai, Y. Lin, H. Wei, X. C. Zeng, and J. Huang, "Defect passivation in hybrid perovskite solar cells using quaternary ammonium halide anions and cations," *Nature Energy*, vol. 2, no. 7, pp. 1–9, Jul. 2017, doi: 10.1038/nenergy.2017.102.

[20] N. K. Noel, A. Abate, S. D. Stranks, E. S. Parrott, V. M. Burlakov, A. Goriely, and H. J. Snaith, "Enhanced photoluminescence and solar cell performance via Lewis base passivation of organic–inorganic lead halide perovskites," *ACS Nano*, vol. 8, no. 10, pp. 9815–9821, Oct. 2014, doi: 10.1021/nn5036476.

[21] Y. Chen, J. Yang, S. Wang, Y. Wu, N. Yuan, and W.-H. Zhang, "Interfacial contact passivation for efficient and stable cesium-formamidinium double-cation lead halide perovskite solar cells," *iScience*, vol. 23, no. 1, Jan. 2020, Art. no. 100762, doi: 10.1016/j.isci.2019.100762.

[22] Z. Ni, C. Bao, Y. Liu, Q. Jiang, W.-Q. Wu, S. Chen, X. Dai, B. Chen, B. Hartweg, Z. Yu, Z. Holman, and J. Huang, "Resolving spatial and energetic distributions of trap states in metal halide perovskite solar cells," *Science*, vol. 367, no. 6484, pp. 1352–1358, Mar. 2020, doi: 10.1126/science.aba0893.

[23] Z. Gao, Y. Wang, D. Ouyang, H. Liu, Z. Huang, J. Kim, and W. C. H. Choy, "Triple interface passivation strategy-enabled efficient and stable inverted perovskite solar cells," *Small Methods*, vol. 4, no. 12, Dec. 2020, Art. no. 2000478, doi: 10.1002/smtd.202000478.

[24] M. Samiee, S. Konduri, B. Ganapathy, R. Kottokkaran, H. A. Abbas, A. Kitahara, P. Joshi, L. Zhang, M. Noack, and V. Dalal, "Defect density and dielectric constant in perovskite solar cells," *Appl. Phys. Lett.*, vol. 105, no. 15, Oct. 2014, Art. no. 153502, doi: 10.1063/1.4897329.

[25] M. M. Salah, M. Abouelatta, A. Shaker, K. M. Hassan, and A. Saeed, "A comprehensive simulation study of hybrid halide perovskite solar cell with copper oxide as HTM," *Semicond. Sci. Technol.*, vol. 34, no. 11, Nov. 2019, Art. no. 115009, doi: 10.1088/1361-6641/ab22e1.

[26] S. Abdelaziz, A. Zekry, A. Shaker, and M. Abouelatta, "Investigating the performance of formamidinium tin-based perovskite solar cell by SCAPS device simulation," *Opt. Mater.*, vol. 101, Mar. 2020, Art. no. 109738, doi: 10.1016/j.optmat.2020.109738.

[27] S. Z. Haider, H. Anwar, and M. Wang, "A comprehensive device modelling of perovskite solar cell with inorganic copper iodide as hole transport material," *Semicond. Sci. Technol.*, vol. 33, no. 3, Mar. 2018, Art. no. 035001, doi: 10.1088/1361-6641/aaa596.

[28] T. S. Sherkar, C. Momblona, L. Gil-Escrig, J. Ávila, M. Sessolo, H. J. Bolink, and L. J. A. Koster, "Recombination in perovskite solar cells: Significance of grain boundaries, interface traps, and defect ions," *ACS Energy Lett.*, vol. 2, no. 5, pp. 1214–1222, May 2017, doi: 10.1021/acsenergylett.7b00236.

[29] F. Izadi, A. Ghobadi, A. Gharaati, M. Minbashi, and A. Hajjiah, "Effect of interface defects on high efficient perovskite solar cells," *Optik*, vol. 227, Feb. 2021, Art. no. 166061, doi: 10.1016/j.ijleo.2020.166061.

[30] W. Zhao, D. Wang, and S. F. Liu, "Sputtered ZnO films as electron transport layers for efficient planar perovskite solar cells," in *Proc. IEEE 7th World Conf. Photovoltaic Energy Convers. (WCPEC) (Joint Conf. 45th IEEE PVSC, 28th PVSEC 34th EU PVSEC)*, Jun. 2018, pp. 539–541, doi: 10.1109/pvsc.2018.8547460.

[31] T. M. Koh, T. Krishnamoorthy, N. Yantara, C. Shi, W. L. Leong, P. P. Boix, A. C. Grimsdale, S. G. Mhaisalkar, and N. Mathews, "Formamidinium tin-based perovskite with low eg for photovoltaic applications," *J. Mater. Chem. A*, vol. 3, no. 29, pp. 14996–15000, 2015, doi: 10.1039/c5ta00190k.

[32] (2021). *PVLighthouse*. Accessed: Jun. 26, 2021. [Online]. Available: Www2.pvlighthouse.com.au and https://www2.pvlighthouse.com.au/resources/photovoltaic%20materials/refractive%20index/refractive%20index.aspx

[33] U. Mandadapu, "Simulation and analysis of lead based perovskite solar cell using SCAPS-1D," *Indian J. Sci. Technol.*, vol. 10, no. 1, pp. 1–8, Jan. 2017, doi: 10.17485/ijst/2017/v11i10/110721.

[34] X. Li, J. Yang, Q. Jiang, W. Chu, D. Zhang, Z. Zhou, and J. Xin, "Synergistic effect to high-performance perovskite solar cells with reduced hysteresis and improved stability by the introduction of na-treated $TiO_2$ and spraying-deposited CuI as transport layers," *ACS Appl. Mater. Interface*, vol. 9, no. 47, pp. 41354–41362, Nov. 2017, doi: 10.1021/acsami.7b14926.

[35] M. D. Stamate, "On the dielectric properties of dc magnetron $TiO_2$ thin films," *Appl. Surf. Sci.*, vol. 218, nos. 1–4, pp. 318–323, 2003, doi: 10.1016/s0169-4332(03)00624-x.

[36] M. M. Salah, K. M. Hassan, M. Abouelatta, and A. Shaker, "A comparative study of different ETMs in perovskite solar cell with inorganic copper iodide as HTM," *Optik*, vol. 178, pp. 958–963, Feb. 2019, doi: 10.1016/j.ijleo.2018.10.052.

[37] H.-J. Du, W.-C. Wang, and J.-Z. Zhu, "Device simulation of lead-free $CH_3NH_3SnI_3$ perovskite solar cells with high efficiency," *Chin. Phys. B*, vol. 25, no. 10, Oct. 2016, Art. no. 108802, doi: 10.1088/1674-1056/25/10/108802.

[38] A. Niemegeers and M. Burgelman, "Numerical modelling of AC-characteristics of CdTe and CIS solar cells," in *Proc. Conf. Rec. 25th IEEE Photovoltaic Spec. Conf.*, May 1996, pp. 901–904, doi: 10.1109/PVSC.1996.564274.

[39] S. Bansal and P. Aryal, "Evaluation of new materials for electron and hole transport layers in perovskite-based solar cells through SCAPS-1D simulations," in *Proc. IEEE 43rd Photovoltaic Spec. Conf. (PVSC)*, Jun. 2016, pp. 0747–0750, doi: 10.1109/PVSC.2016.7749702.

[40] F. Hao, C. C. Stoumpos, R. P. H. Chang, and M. G. Kanatzidis, "Anomalous band gap behavior in mixed Sn and Pb perovskites enables broadening of absorption spectrum in solar cells," *J. Amer. Chem. Soc.*, vol. 136, no. 22, pp. 8094–8099, 2014, doi: 10.1021/ja5033259.

[41] Z. Zhao, F. Gu, Y. Li, W. Sun, S. Ye, H. Rao, Z. Liu, Z. Bian, and C. Huang, "Mixed-organic-cation tin iodide for lead-free perovskite solar cells with an efficiency of 8.12%," *Adv. Sci.*, vol. 4, no. 11, Nov. 2017, Art. no. 1700204, doi: 10.1002/advs.201700204.

[42] C. Kim, T. D. Huan, S. Krishnan, and R. Ramprasad, "A hybrid organic-inorganic perovskite dataset," *Sci. Data*, vol. 4, no. 1, Dec. 2017, Art. no. 170057, doi: 10.1038/sdata.2017.57.

[43] L. M. Herz, "Charge-carrier mobilities in metal halide perovskites: Fundamental mechanisms and limits," *ACS Energy Lett.*, vol. 2, no. 7, pp. 1539–1548, May 2017, doi: 10.1021/acsenergylett.7b00276.

[44] T. Minemoto and M. Murata, "Device modeling of perovskite solar cells based on structural similarity with thin film inorganic semiconductor solar cells," *J. Appl. Phys.*, vol. 116, no. 5, Aug. 2014, Art. no. 054505, doi: 10.1063/1.4891982.

[45] H. Shen, D. A. Jacobs, Y. Wu, T. Duong, J. Peng, X. Wen, X. Fu, S. K. Karuturi, T. P. White, K. Weber, and K. R. Catchpole, "Inverted hysteresis in $CH_3NH_3PbI_3$ solar cells: Role of stoichiometry and band alignment," *J. Phys. Chem. Lett.*, vol. 8, no. 12, pp. 2672–2680, Jun. 2017, doi: 10.1021/acs.jpclett.7b00571.

[46] S. J. Lee, S. S. Shin, J. Im, T. K. Ahn, J. H. Noh, N. J. Jeon, S. I. Seok, and J. Seo, "Reducing carrier density in formamidinium tin perovskites and its beneficial effects on stability and efficiency of perovskite solar cells," *ACS Energy Lett.*, vol. 3, no. 1, pp. 46–53, Jan. 2018, doi: 10.1021/acsenergylett.7b00976.

[47] H.-H. Fang, S. Adjokatse, S. Shao, J. Even, and M. A. Loi, "Long-lived hot-carrier light emission and large blue shift in formamidinium tin triiodide perovskites," *Nature Commun.*, vol. 9, no. 1, p. 243, Dec. 2018, doi: 10.1038/s41467-017-02684-w.

[48] M. Burgelman, K. Decock, S. Khelifi, and A. Abass, "Advanced electrical simulation of thin film solar cells," *Thin Solid Films*, vol. 535, pp. 296–301, May 2013, doi: 10.1016/j.tsf.2012.10.032.

[49] A. Haddout, A. Raidou, and M. Fahoume, "Influence of the layer parameters on the performance of the CdTe solar cells," *Optoelectron. Lett.*, vol. 14, no. 2, pp. 98–103, Mar. 2018, doi: 10.1007/s11801-018-7229-4.

[50] R. Ishikawa, S. Watanabe, S. Yamazaki, T. Oya, and N. Tsuboi, "Perovskite/graphene solar cells without a hole-transport layer," *ACS Appl. Energy Mater.*, vol. 2, no. 1, pp. 171–175, Jan. 2019, doi: 10.1021/acsaem.8b01606.

[51] W. J. Yang, Z. Q. Ma, X. Tang, C. B. Feng, W. G. Zhao, and P. P. Shi, "Internal quantum efficiency for solar cells," *Sol. Energy*, vol. 82, no. 2, pp. 106–110, Feb. 2008, doi: 10.1016/j.solener.2007.07.010.

[52] W. Abdelaziz, A. Shaker, M. Abouelatta, and A. Zekry, "Possible efficiency boosting of non-fullerene acceptor solar cell using device simulation," *Opt. Mater.*, vol. 91, pp. 239–245, May 2019, doi: 10.1016/j.optmat.2019.03.023.

[53] W. Shockley and W. T. Read, Jr., "Statistics of the recombinations of holes and electrons," *Phys. Rev.*, vol. 87, no. 5, pp. 835–842, 1952, doi: 10.1103/physrev.87.835.

[54] R. N. Hall, "Electron-hole recombination in germanium," *Phys. Rev.*, vol. 87, no. 2, p. 387, 1952, doi: 10.1103/physrev.87.387.

[55] D. L. Scharfetter and H. K. Gummel, "Large-signal analysis of a silicon Read diode oscillator," *IEEE Trans. Electron Devices*, vol. ED-16, no. 1, pp. 64–77, Jan. 1969, doi: 10.1109/t-ed.1969.16566.

[56] H. K. Gummel, "A self-consistent iterative scheme for one-dimensional steady state transistor calculations," *IEEE Trans. Electron Devices*, vol. ED-11, no. 10, pp. 455–465, Oct. 1964, doi: 10.1109/t-ed.1964.15364.

[57] M. Boumaour, S. Sali, S. Kermadi, L. Zougar, A. Bahfir, and Z. Chaieb, "High efficiency silicon solar cells with back ZnTe layer hosting IPV effect: A numerical case study," *J. Taibah Univ. Sci.*, vol. 13, no. 1, pp. 696–703, Dec. 2019, doi: 10.1080/16583655.2019.1623476.

[58] H. J. Pauwels and G. Vanhoutte, "The influence of interface state and energy barriers on the efficiency of heterojunction solar cells," *J. Phys. D, Appl. Phys.*, vol. 11, no. 5, pp. 649–667, Apr. 1978, doi: 10.1088/0022-3727/11/5/009.

[59] J. M. Ball and A. Petrozza, "Defects in perovskite-halides and their effects in solar cells," *Nature Energy*, vol. 1, no. 11, pp. 1–13, Nov. 2016, doi: 10.1038/nenergy.2016.149.

[60] H. Zhu, K. Miyata, Y. Fu, J. Wang, P. P. Joshi, D. Niesner, K. W. Williams, S. Jin, and X.-Y. Zhu, "Screening in crystalline liquids protects energetic carriers in hybrid perovskites," *Science*, vol. 353, no. 6306, pp. 1409–1413, Sep. 2016, doi: 10.1126/science.aaf9570.

[61] R. Su, Z. Xu, J. Wu, D. Luo, Q. Hu, W. Yang, X. Yang, R. Zhang, H. Yu, T. P. Russell, Q. Gong, W. Zhang, and R. Zhu, "Dielectric screening in perovskite photovoltaics," *Nature Commun.*, vol. 12, no. 1, pp. 1–11, Dec. 2021, doi: 10.1038/s41467-021-22783-z.

[62] R. Brakkee and R. M. Williams, "Minimizing defect states in lead halide perovskite solar cell materials," *Appl. Sci.*, vol. 10, no. 9, p. 3061, Apr. 2020, doi: 10.3390/app10093061.

[63] W. Tress, "Perovskite solar cells on the way to their radiative efficiency limit–insights into a success story of high open-circuit voltage and low recombination," *Adv. Energy Mater.*, vol. 7, no. 14, Jul. 2017, Art. no. 1602358, doi: 10.1002/aenm.201602358.

[64] T. Zhao, W. Shi, J. Xi, D. Wang, and Z. Shuai, "Intrinsic and extrinsic charge transport in $CH_3NH_3PbI_3$ perovskites predicted from first-principles," *Sci. Rep.*, vol. 6, no. 1, Feb. 2016, Art. no. 19968, doi: 10.1038/srep19968.

[65] H. Kim, K.-G. Lim, and T.-W. Lee, "Planar heterojunction organometal halide perovskite solar cells: Roles of interfacial layers," *Energy Environ. Sci.*, vol. 9, no. 1, pp. 12–30, 2016, doi: 10.1039/c5ee02194d.

[66] M. Yousefi, M. Minbashi, Z. Monfared, N. Memarian, and A. Hajjiah, "Improving the efficiency of CZTSSe solar cells by engineering the lattice defects in the absorber layer," *Sol. Energy*, vol. 208, pp. 884–893, Sep. 2020, doi: 10.1016/j.solener.2020.08.049.

[67] M. Mousa, F. Z. Amer, R. I. Mubarak, and A. Saeed, "Simulation of optimized high-current tandem solar-cells with efficiency beyond 41%," *IEEE Access*, vol. 9, pp. 49724–49737, 2021, doi: 10.1109/access.2021.3069281.

[68] M. S. Salem, A. Zekry, A. Shaker, M. Abouelatta, and T. M. Abdolkader, "Performance enhancement of a proposed solar cell microstructure based on heavily doped silicon wafers," *Semicond. Sci. Technol.*, vol. 34, no. 3, Mar. 2019, Art. no. 035012, doi: 10.1088/1361-6641/ab0078.

[69] N. Gamal, S. H. Sedky, A. Shaker, and M. Fedawy, "Design of lead-free perovskite solar cell using $Zn_{1-x}Mg_xO$ as ETL: SCAPS device simulation," *Optik*, vol. 242, Sep. 2021, Art. no. 167306, doi: 10.1016/j.ijleo.2021.167306.

[70] M. Abdelnaby, A. Zekry, F. Elakkad, and H. Ragaie, "Dependence of dark current on zinc concentration in $Zn_xCd_{1-x}S$/ZnTe heterojunctions," *Sol. Energy Mater. Sol. Cells*, vol. 29, no. 2, pp. 97–108, 1993, doi: 10.1016/0927-0248(93)90067-d.

**MARWA SAYED SALEM BASYONI** was born in Gedda, Saudi Arabia, in 1979. She received the B.Sc. degree from the Electronics and Communications Engineering Department, Faculty of Engineering, Ain Shams University, Cairo, Egypt, in 2002, and the master's and Ph.D. degrees in renewable energy, especially in solar cells from Ain Shams University, in 2006 and 2013, respectively. She worked as a Research Assistant with the Faculty of Engineering, Ain Shams University, from 2003 to 2013. She is currently an Assistant Professor with the Computer Science and Engineering College, University Ha'il, Ha'il, Saudi Arabia. Her research interests include VLSI design, MEMS technology, nanotechnology, renewable energy, solar cell, PV systems, semiconductor physics, and simulation and modeling of power devices.

**MOSTAFA M. SALAH** received the bachelor's degree from Future University in Egypt and the M.Sc. degree from Ain Shams University, where he is currently pursuing the Ph.D. degree with the Electronics and Communications Engineering Department, Faculty of Engineering. He is also an Assistant Lecturer with the Electrical Engineering Department, Future University in Egypt.

**MOHAMED MOUSA** received the bachelor's degree from Future University in Egypt, and the M.Sc. degree from Ain Shams University. He is currently pursuing the Ph.D. degree with the Electronics and Communications Engineering Department, Faculty of Engineering, Helwan University. He is also an Assistant Lecturer with the Electrical Engineering Department, Future University in Egypt.

**AHMED SHAKER** was born in Cairo, Egypt. He received the M.Sc. and Ph.D. degrees from Ain Shams University, Cairo, in 2003 and 2010, respectively. He has been with the Engineering Physics Department, Faculty of Engineering, Ain Shams University, since 1997, where he is currently an Associate Professor. He joined North Carolina State University, as a Postdoctoral Researcher, from August 2020 to February 2021, where he was involved in the fabrication and characterization of GaN-based LEDs. His research interests include simulation and modeling of semiconductor power devices, solar cells, LEDs, 3-D detectors, and nanoscale devices, including TFETs and CNTFETs.

**ABDELHALIM ZEKRY** (Member, IEEE) received the B.Sc. and M.Sc. degrees from Cairo University, Egypt, in 1969 and 1973, respectively, and the Ph.D. degree from TU Berlin, in 1981. He worked as a Scientific Coworker with TU Berlin. He was a Staff Member at several rewarded universities. He is currently a Professor in electronics with the Faculty of Engineering, Ain Shams University, Cairo, Egypt. He has supervised over 100 master's thesis and 30 Ph.D. dissertations. He has also authored or coauthored over 240 conference and periodical papers. His current research interests include the field of microelectronics and electronic applications, including communications and photovoltaics. He received several prizes for the acknowledgment of his outstanding research and teaching performance.

**MOHAMED ABOUELATTA** was born in Cairo, Egypt. He received the B.Sc. and M.Sc. degrees in electronics and communication engineering from Ain Shams University (ASU), in 1996 and 2001, respectively, and the joint Ph.D. degree from Ain Shams University and the National Institute of Applied Sciences of Lyon (INSA Lyon), France, in 2010. He is currently a Professor with the Faculty of Engineering, ASU. His research interests include modeling, design, and characterization of power devices, designing of smart power integrated circuits, nanodevices, photovoltaic, and 3-D CMOS heterogeneous integrated circuits.

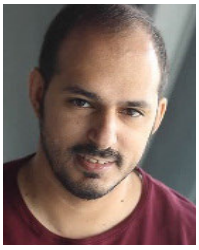

**MOHAMMAD T. ALSHAMMARI** received the B.S. degree in computer science education from the University of Ha'il, Saudi Arabia, in 2007, and the M.Sc. and Ph.D. degrees in computer science from the University of Birmingham, U.K., in 2011 and 2016, respectively. He has been an Associate Professor with the College of Computer Science and Engineering, University of Ha'il, since May 2021.

**KAWTHER A. AL-DHLAN** is currently an Associate Professor in computer science. She has ten years' experience in data science and more than 25 years in academic fields. She also teaches at the University of Hail, Saudi Arabia. Moreover, she is interested in many branches of CS, such as security, cloud computing, and deep learning.

**CHRISTIAN GONTRAND** was born in Montpellier, France. He received the M.Sc., Ph.D., and State Doctorate degrees in electronics from the Universiteì des Sciences et Techniques du Languedoc, Montpellier, in 1977, 1982, and 1987, respectively. From 1982 to 1984, he worked with Thomson "Laboratoire Central de Recherche (LCR)" Orsay, where his areas of interest include theoretical (electrical transport) and experimental (noise) of microwave devices (TEGFETs/HEMTs). Since 1988, he is with the Laboratoire de Physique de la Matie're (LPM/INSA), Villeurbanne, as a Research Assistant Professor. From 1988 to 1996, he was the technical charge of the new "Centre de Microeìlectronique de la Reìgion Lyonnaise (CIMIRLY)" and worked on new RF compatible silicon devices, in collaboration with the Centre National des Etudes en Telecommunication (CNET), Meylan. From 1997 to 2001, as a Professor in semiconductor devices and circuits, he was the Head of the team "Smart System Integration," Centre de Geìnie Electrique de Lyon (CEGELY). In September 2001, he created the team "Radiofrequency Devices, Circuits and Systems" of LPM/INL. His fields of interest are noises or parasitic disturbances in heterogenic 2-D or 3-D RF circuits and systems. Since 2016, he has been working with INSA—Fès, Euro-Mediterranean University, on firmware RF field and smart system integration.